

# Assessment of Predictive Capability of Aeromechanics Methods

William G. Bousman  
 Quercus Associates SL  
 321 Arlington Way  
 Menlo Park, California 94025

Thomas Norman  
 Aeromechanics Branch  
 NASA Ames Research Center  
 Moffett Field, California 94035

## ABSTRACT

A technique is described, based on simple statistics, that can be used to assess the accuracy of analytical predictions compared to measurements. It is demonstrated that the approach can be applied to a broad range of problems in the area of helicopter aeromechanics, including hover and forward flight performance, blade aerodynamic and structural loads, vibratory forces, stability, and rotorcraft icing. The method described has both strengths and weaknesses and these are shown with examples and discussed. It is also shown that there is currently a hierarchy of accuracy in aeromechanics problems, ranging from the necessarily accurate methods for performance prediction to the inaccurate and untrustworthy calculations of fixed-system vibration.

### NOMENCLATURE

$A$	rotor disk area, ft <sup>2</sup>	$P$	power, HP
$C_{CM}$	chord bending moment coefficient, $M_C / \rho AV_T^2 R$	$P_H$	power to hover, HP
$C_{FM}$	chord bending moment coefficient, $M_F / \rho AV_T^2 R$	$R$	blade radius, in
$C_P$	power coefficient, $P / \rho AV_T^3$ or pressure coefficient	$r$	section radius, in
$C_T$	thrust coefficient, $T / \rho AV_T^2$	$S_e$	standard error of estimate, linear regression
$C_{TM}$	chord bending moment coefficient, $M_T / \rho AV_T^2 R$	$T$	rotor thrust, lb
$C_W$	weight coefficient, $GW / \rho AV_T^2$	$V_H$	ideal induced velocity in hover, ft/sec
$c_m$	section pitching moment coefficient	$V_{ROC}$	vertical rate of climb, ft/sec
$c_n$	section normal force coefficient	$V_T$	rotor tip speed, ft/sec
$M_C$	chord bending moment, in-lb	$\mu$	advance ratio
$M$	section Mach number	$\rho$	density of air, slugs/ft <sup>3</sup>
$M_F$	flap bending moment, in-lb	$\sigma$	standard deviation or rotor solidity
$M_T$	torsion moment, in-lb		
$M_{tip}$	tip Mach number		
$GW$	gross weight, lb		
$m$	slope, linear regression		

### INTRODUCTION

Under NASA's Subsonic Rotary Wing (SRW) Project, a detailed assessment of the predictive accuracy of numerous analytical methods has been made, including those methods dealing with aeromechanics, acoustics, experimental methods, flight dynamics and control, propulsion, and structures and materials. Within the general area of aeromechanics, this assessment has been divided into two parts, the first dealing with classical methods embodied in comprehensive analyses and the second dealing with Computational Fluid Dynamics (CFD) with a particular emphasis on coupled CFD/CSD methods and Navier-Stokes representations of the aerodynamic forces. The present paper addresses the

---

Presented at the AHS Specialist's Conference on Aeromechanics, San Francisco, CA, Jan. 23-25, 2008. Copyright 2008 by the American Helicopter Society International, Inc. All rights reserved.

first part of the aeromechanics assessment, that dealing with classical methods.

Progress in the aeromechanics disciplines over the last 70 to 80 years has been substantial, yet there have been few attempts at a quantitative assessment of analytical methods (Refs. 1-3). Some 30 plus years ago, at the Dynamic Specialists Meeting at Ames Research Center, Dick Bennett said “. . . correlation, like beauty, is in the eye of the beholder.” (Ref. 4). These words, a fine example of Dr. Bennett’s wit, have lingered in the engineering community for decades. Yet his statement has been taken out of context. Dick used these words as an example of fuzzy thinking and in the next sentence he stated “So we must come up with a good definition, a workable definition of correlation.”

The primary purpose of this paper is to present one approach to quantitative correlation, using the work that has been done under NASA’s SRW Project. Beyond that primary purpose, it will also be shown that the use of quantitative correlation provides insight into the accuracy of present analytical methods when applied over a range of aeromechanics problems.

### METHODOLOGY FOR QUANTITATIVE CORRELATION

A standardized approach to the quantitative assessment of predictive accuracy of analytical methods is described here. The basic approach is to plot the calculation of an appropriate parameter as a function of its measurement. Exact correlation is obtained if all the calculated and measured points lie on a 45° line. This approach is illustrated in Figs. 1 and 2. Figure 1 shows the measured and calculated aircraft power coefficients,  $C_p$ , for advance

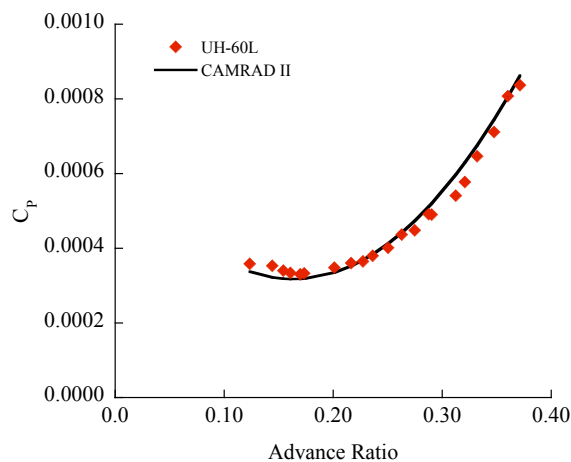


Figure 1. UH-60L with standard blades. Power coefficient as a function of advance ratio;  $C_W/\sigma = 0.0787$  (Ref. 5).

ratios from about 0.15 to 0.35 for a UH-60L with standard blades. The aircraft weight coefficient in this case,  $C_W/\sigma$ , is about 0.079. The calculations have been made using CAMRAD II (Ref. 5). A qualitative examination of Fig. 1 shows that there is fairly good agreement between analysis and data, but the power is underpredicted at low speeds and overpredicted for  $0.25 \leq \mu \leq 0.35$ . Figure 2 shows the calculated  $C_p$  as a function of the measured  $C_p$  for the data. A linear regression line is calculated for the correlation points and is shown as a solid line bracketed by dashed lines that represent the scatter of the data. The scatter is indicated by  $\pm S_e$  (the standard error of estimate, which is equivalent to  $\pm 1\sigma$ ). The scatter in this case is a little more than 1% (based on the ordinate scale), which is typical of better performance calculations. At low power coefficients there is an underprediction in Fig. 2, whereas at high power coefficients there is an overprediction, as was noted for Fig. 1. The slope of the linear regression line is 1.093 in this case. In this assessment approach, slopes greater than 1.0 are considered an overprediction and slopes less than 1.0 are an underprediction.

The scatter in the correlation in the example in Fig. 2 is presumably caused by measurement errors. But the difference in the slope of the regression line, in this case an overprediction, may be caused by errors in analysis or measurement.

In this example, the power coefficient varies over a range of about 2.5x, which provides a reasonable assessment of the correlation. If this range or ratio were close to 1.0x, the lack of variation would be so limited that the regression fit would be meaningless. In the example shown in Fig. 1, the

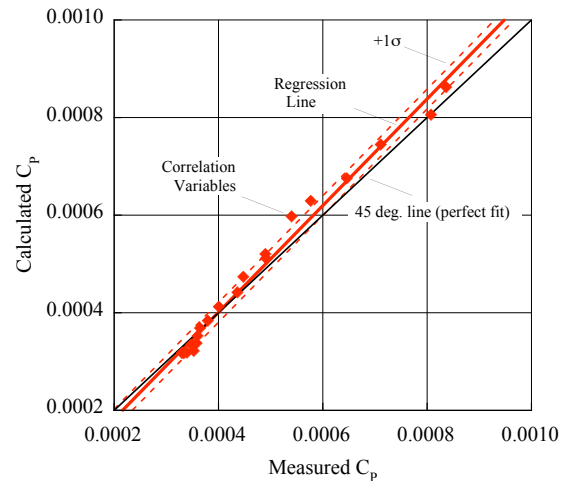


Figure 2. Predictive accuracy of CAMRAD II for UH-60L with standard blades for  $C_W/\sigma = 0.0787$ ;  $m = 1.093$ ,  $S_e = \pm 1\%$  (Ref. 5).

variation in the power coefficient is caused by changes in airspeed, but it is generally not important what the source of the variation is.

In the example of Fig. 2, the scatter is quite low, and quantitatively the predictive accuracy is usefully judged by the slope,  $m = 1.093$ . But in other cases, as will be shown below, the scatter may be much larger and this scatter may be more significant in assessing the accuracy of the prediction. Moreover, in other cases there will be a noticeable offset in values and this offset may be more important than either the slope or scatter.

It is useful in many cases to include additional independent variables and group comparisons together. Thus, for the UH-60L flight test data, power coefficient data at other weight coefficients (airspeed sweeps) can be used, and the data are combined or grouped together, which may provide a better test, as suggested by Fig. 3. In this example, data and calculations from four airspeed sweeps are combined and the overall slope is 1.024, indicating a calculation accuracy of +2.4%.

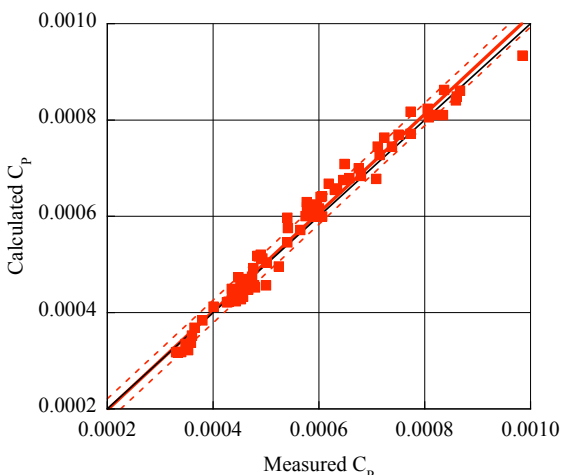


Figure 3. Predictive accuracy of CAMRAD II for UH-60L with standard blade for four weight coefficients (Ref. 5);  $m = 1.024$ ,  $S_e = \pm 2\%$ .

The combined analysis of the four airspeed sweeps in Fig. 3 is perhaps a better estimate of the predictive accuracy of CAMRAD II, since a wider parameter variation is used in the assessment. But in some cases, combining data sets can obscure trends that may be important. Table 1 shows the slopes and scatter for the four airspeed sweeps used in Fig. 3. For the three lower  $C_W/\sigma$  values, the overprediction varies from 0.3% to 9.3%. But for the highest weight coefficient, there is a 15.2% underprediction. The scatter is relatively unchanged, but the change in slope suggests that the calculation has degraded at high blade loading, perhaps because of dynamic stall.

Table 1. Predictive accuracy of CAMRAD II for UH-60L with standard blade for four weight coefficients (Ref. 5).

$C_W/\sigma$	$m$	$\pm S_e, \%$
0.0787	1.093	1.4
0.0981	1.003	1.6
0.1029	1.034	1.4
0.1211	0.848	1.7

The choice of a relevant parameter for quantitative correlation can be difficult. For performance, the choice of the power required at a single test point is straightforward. But for that same test point, it is not so clear how to represent the blade aerodynamic or structural loads. Figure 4 compares the measured and predicted nondimensional vibratory

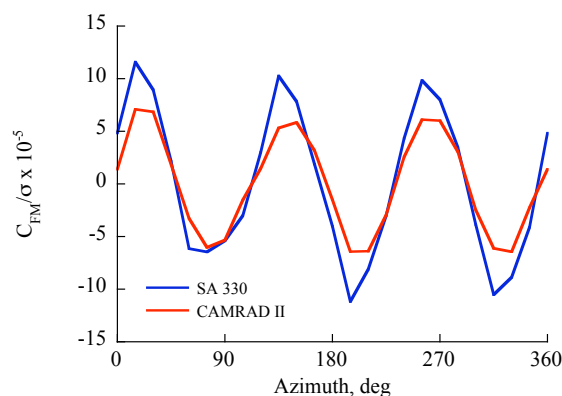


Figure 4. SA 330 (Puma) nondimensional vibratory flap bending moment as a function of blade azimuth at  $0.46R$  and  $\mu = 0.362$  (Ref. 6).

flap bending moment for the research Puma (Ref. 6). What number or numbers are the best choice to represent this correlation? The peak-to-peak loads describe the total amplitude of the flap bending moment, but do not describe the frequency content, either in amplitude (generally) or phase. The approach used here is to examine the predictive accuracy by sampling the data every 15 deg., which represents the frequency content of the measured time history. Thus, the blade azimuth is treated as the independent variable. The resulting linear regression for this example is shown in Fig. 5. The vibratory loads in this case are underpredicted by about 35%, which is also clearly seen in the time history in Fig. 4. The scatter is about  $\pm 7\%$ , which is an increase from that observed in the UH-60L performance results in Fig. 3, but as will be shown below is quite good for structural load prediction.

But what happens when there is a phase shift in the structural loads? Figure 6 shows a correlation

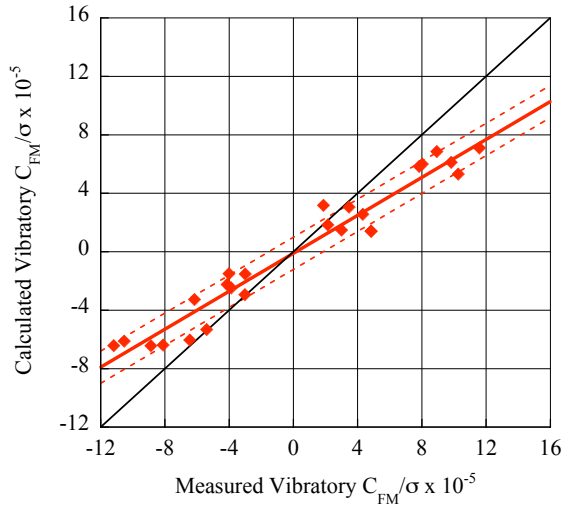


Figure 5. SA 330 (Puma) linear regression of nondimensional vibratory flap bending moment at  $0.46R$  and  $\mu = 0.362$  (Ref. 6);  $m = 0.649$ ,  $S_e = \pm 7\%$ .

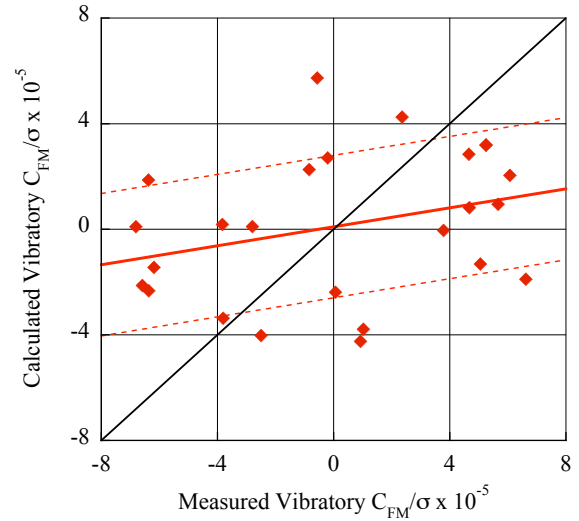


Figure 7. UH-60A linear regression of nondimensional vibratory flap bending moment at  $0.50R$  and  $\mu = 0.368$  (Ref. 6);  $m = 0.180$ ,  $S_e = \pm 17\%$ .

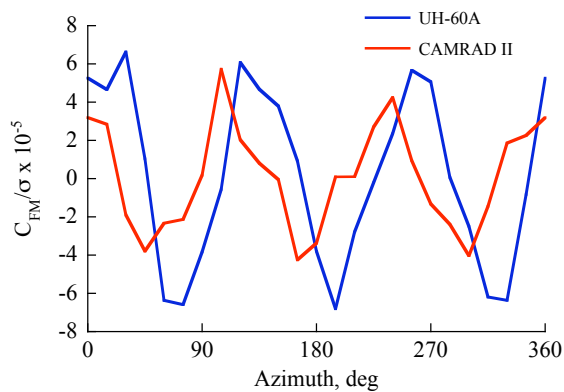


Figure 6. UH-60A nondimensional vibratory flap bending moment as a function of blade azimuth at  $0.50R$  and  $\mu = 0.368$  (Ref. 6).

case for the vibratory flap bending moment for the UH-60A that includes a substantial phase shift. The predicted amplitude in this case appears to be about 75% of the measurement, but the phase difference has a severe effect on the linear regression fit as shown in Fig. 7. Because of the phase difference the scatter is increased and the slope of the linear regression fit is essentially meaningless. The examples shown in Figs. 6 and 7 provide a warning that the present methodology is sensitive to some aspects of correlation, particularly phase differences (which may be a good thing).

### Aeromechanics Topics

The remainder of this paper will look at a wide range of aeromechanics topics using the quantitative correlation approach described here. Topics range from basic rotorcraft performance, both in hover and forward flight, aerodynamic loads on the blade and fuselage, structural loads, vibration, and rotor stability along with a few miscellaneous topics. In selecting these topics, only results from the published literature have been used. An effort has been made to use data sets where one analysis has been used for many different experimental cases and the investigators have applied their method in a uniform manner.

Although a broad range of topics are included here, the predictions of only a limited number of comprehensive analyses have been examined. There are many other codes that are available, and the examination of their predictive capability would be valuable. Moreover, the examination of additional cases would provide a better evaluation of the applicability of the present method.

In some cases words may be used here such as error, discrepancy, or difference, and these words are used interchangeably. But it is important to recognize that differences between measurement and calculation may be caused by errors in the calculation, errors in the measurements, or errors in both. When reasonably good correlation is obtained, as is the case currently for flight performance, it will be pointed out that improvement in calculation accuracy cannot be obtained until significant

improvements are made in measurement accuracy. But in other cases, the need for improvement lies with analysis.

### Hover Performance

Felker et al. (Ref. 7) applied the hover performance code EHPIC to a broad range of rotor tests, including four main rotors, two tail rotors, and three tiltrotors. The EHPIC code is a lifting surface analysis that uses a free wake. Drag is determined using table lookup. More or less typical of the basic hover performance data used in Ref. 7, Fig. 8 shows the measured power coefficient as a function of thrust coefficient for the Boeing prototype YUH-61A main rotor tested on a whirl tower along with the EHPIC code prediction (consult Ref. 7 for

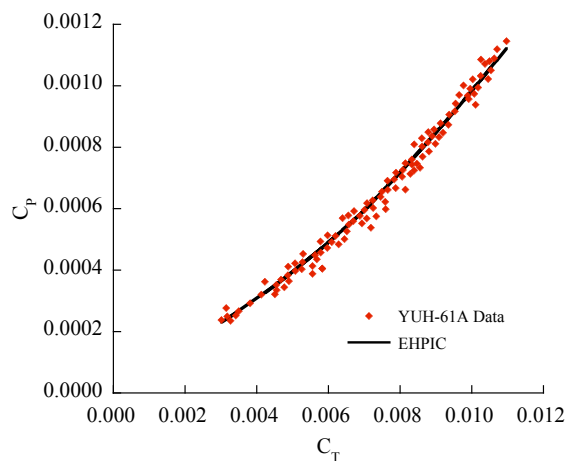


Figure 8.  $C_p$  as a function of  $C_T$  for the Boeing YUH-61A main rotor tested on a whirl tower compared to EHPIC code (Ref. 7).

the original data sources). The range of power coefficient values in this case is about 4.9x.

The accuracy of the EHPIC code for four main rotors is shown in Fig. 9. For the combined analysis, the underprediction is about 1.5% and the scatter is low. The four rotors analyzed include a two-bladed rotor with significant taper that was tested about 1958 and is referred to as the TN 4357 rotor (TN 4357 was the NACA technical note wherein the data were published). This rotor, 53.6-feet in diameter, was tested on a whirl tower with a height-to-diameter ratio of 0.78. Because of ground plane effects, the data were corrected (about 5%). Two different tip Mach numbers are included in the data set. The second data set was for a three-bladed rotor, tested about 1951, and is referred to as the TN 2277 rotor. This rotor was untapered and had a 38-foot diameter. As with the two-bladed test, two different tip Mach numbers were tested. The third data set was

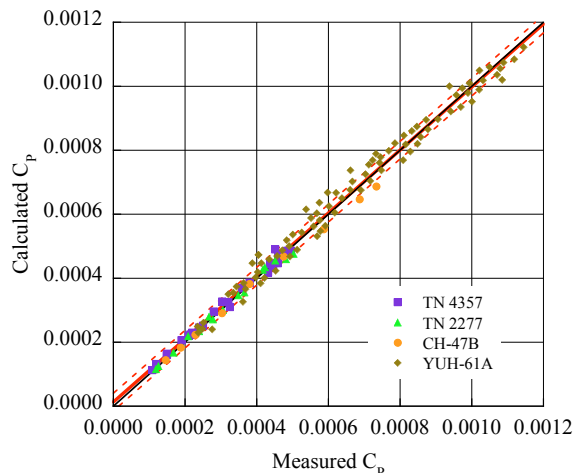


Figure 9. Accuracy of EHPIC hover prediction for four main rotors (Ref. 7);  $m = 0.985$ ,  $S_e = \pm 2\%$ .

a CH-47B rotor tested on a whirl tower, also with three blades. The fourth data set was for the four-bladed YUH-61A rotor, also tested on a whirl tower (see Fig. 8). Table 2 compares the accuracy metrics for the four data sets. The hover performance is underpredicted for all main rotors, ranging from 7.2% to 2.7%.

Table 2. Accuracy of EHPIC for hover performance of four main rotors (Ref. 7).

Main Rotor	Blade No.	$m$	$\pm S_e, \%$
TN 4357	2	0.973	1.0
TN 2277	3	0.971	0.9
CH-47B	3	0.927	1.3
YUH-61A	4	0.966	2.6

Two untwisted tail rotors, the Bell Model 222 and Model 214A, were tested on a tail rotor test stand. The accuracy of the EHPIC code for these rotor tests is shown in Fig. 10. There are two data sets for the Bell 214A, one at a tip Mach number,  $M_{tip}$ , of 0.69 and the other at  $M_{tip} = 0.73$ . Hence, the analysis here is for the three combined data sets. The combined analysis shows about a 10% overprediction of power but there is a wide variation of predictive accuracy for these two tail rotors as indicated in Table 3. There is little scatter in the individual data sets.

The EHPIC accuracy for the three tiltrotor data sets is shown in Fig. 11. The XV-15 rotor is the development rotor flown on the XV-15 over a number of years. The Advanced Technology Blade (ATB) rotor was developed by Boeing Helicopters and underwent limited flight tests on the XV-15. The

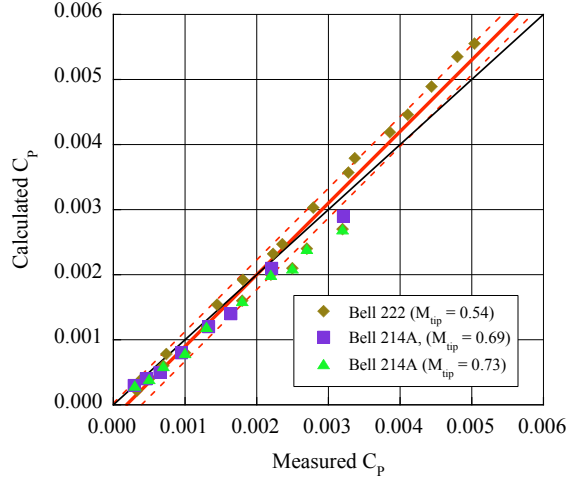


Figure 10. Accuracy of EHPIC hover prediction for two tail rotors (Ref. 7);  $m = 1.100$ ,  $S_e = \pm 4\%$ .

Table 3. Accuracy of EHPIC for hover performance of two tail rotors (Ref. 7).

Tail Rotor	$M_{tip}$	$m$	$\pm S_e, \%$
Bell 222	0.54	1.123	0.9
Bell 214A	0.69	0.919	0.7
Bell 214A	0.73	0.847	0.7

scaled V-22 tiltrotor, an early version of the Navy's Osprey tiltrotor, was tested extensively at NASA Ames Research Center. All three of these highly twisted rotors were tested on a horizontal test stand at Ames. The combined analysis shows an overprediction of 7.2%, but the scatter is quite low. The accuracies for the individual tests are shown in Table 4 and the predictions for the three rotors are similar.

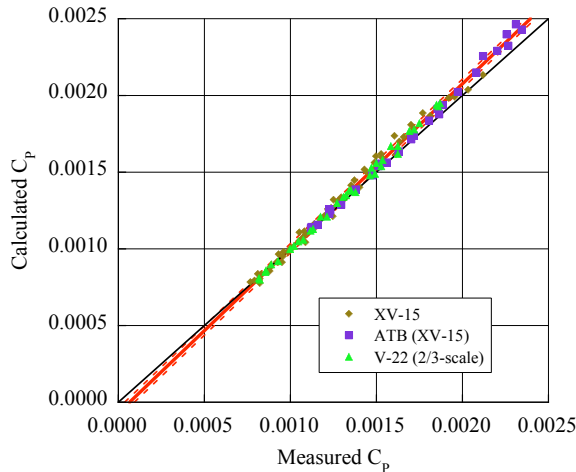


Figure 11. Accuracy of EHPIC hover prediction for three tiltrotors (Ref. 7);  $m = 1.072$ ,  $S_e = \pm 1\%$ .

Table 4. Accuracy of EHPIC for hover performance of three tiltrotors (Ref. 7).

Tiltrotor	$m$	$\pm S_e, \%$
XV-15	1.067	1.4
ATB (XV-15)	1.095	1.1
V-22 (0.67-scale)	1.080	0.8

The CHARM comprehensive code, a follow-on to the EHPIC code, also uses lifting surface theory and a free-wake analysis. Wachspress et al. (Ref. 8) have examined four different sets of hover performance data, including two main rotor hover data sets, a model-scale data set, and a tiltrotor data set. The dependent variable in these cases is Figure of Merit rather than power coefficient. The range of Figure of Merit values here is 2.4x, which is about half the range used in the EHPIC hover performance evaluation. An example of these performance data, in this case the 0.17-scale model UH-60A data that were not available for the EHPIC evaluation in 1988, is shown in Fig. 12. The

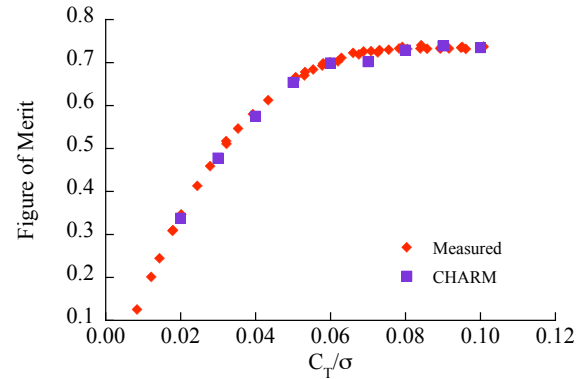


Figure 12. Figure of Merit as a function of  $C_T/\sigma$  for Sikorsky Aircraft 0.17-scale UH-60A rotor compared to CHARM code (Ref. 8).

combined accuracy analysis for the four data sets are shown in Fig. 13. The Figure of Merit is underpredicted by 2.2% and the scatter is low. An examination of the individual hover data sets, as shown in Table 5, shows a wide variation in accuracy. Moreover, two of these data sets were examined with the EHPIC code 15 years earlier and very different results were obtained. But the overall accuracy is quite similar.

Kocurek et al. (Ref. 2) evaluated the Bell Helicopter Textron hover prediction methodology in the late 1970s. Their analysis used a lifting surface method with an empirical wake model. They

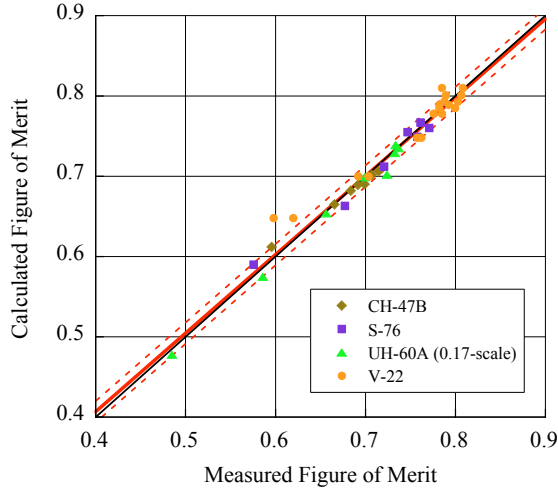


Figure 13. Accuracy of CHARM hover prediction for four hover performance data sets (Ref. 8);  $m = 0.978$ ,  $S_e = \pm 2\%$ .

Table 5. Accuracy of CHARM for hover performance of four data sets (Ref. 8).

Rotor	Blade No.	$m$	$\pm S_e, \%$
CH-47B	3	0.794	0.3
S-76	4	0.932	1.2
UH-60A (0.17 scale)	4	1.007	0.9
V-22 (0.67 scale)	3	0.815	1.3

evaluated a number of isolated rotor data sets, but also included flight test results from 13 helicopters. Thus, their analysis calculated not only hover performance, but also fuselage download, tail rotor power, accessory losses, and transmission losses. They found that the differences between measured and predicted power varied for the most part between  $-3.2$  and  $+3.2\%$ . It appears that predictive accuracy has not substantially changed in the last 30 years or so. At the beginning of this paper, it was stated that the quantitative evaluation of predictive accuracy may benefit from comparisons with multiple data sets. But as analytical methods become more accurate, the use of multiple data sets may be counterproductive because of unknown errors in some of these data sets.

#### Vertical Rate-of-Climb

The U.S. Army requires a minimum maneuver capability at its design hover ceiling, usually expressed as a 500 ft/min vertical rate-of-climb (VROC). Harris (Ref. 9) has pointed out that the accuracy of power prediction for a vertical climb

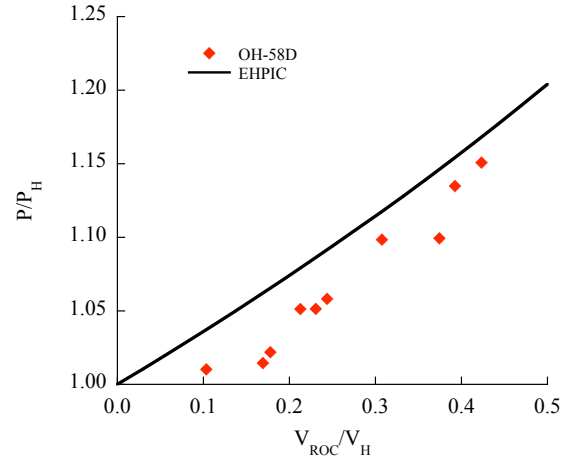


Figure 14. OH-58D vertical rate-of-climb, power ratio as a function of nondimensional climb rate (Ref. 7).

is poor. He included flight test data in Ref. 9 from the OH-58D development program and these data have been used by Felker et al. (Ref. 7) to examine the accuracy of the EHPIC code for VROC prediction. Figure 14 shows the power ratio in a vertical climb as a function of the nondimensional climb rate. At these low climb rates (a  $V_{ROC}/V_H \sim 0.3$  is equivalent to a 500 ft/min climb), the EHPIC code overpredicts the power required. This is shown more clearly in Fig. 15, which shows the linear regression

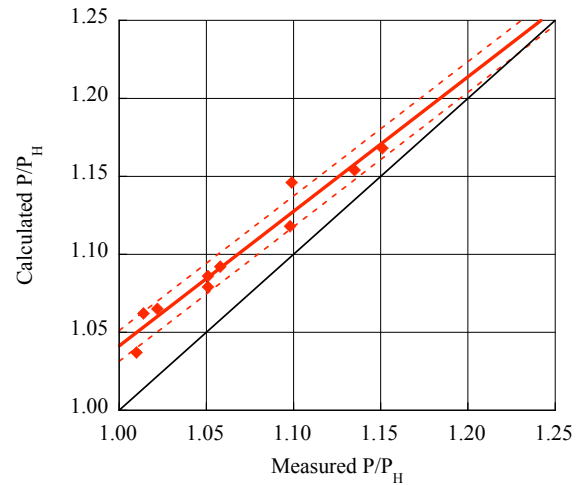


Figure 15. Accuracy of EHPIC vertical rate-of-climb prediction for OH-58D (Ref. 7);  $m = 0.862$ ,  $S_e = \pm 1\%$ .

fit to the data. The slope of the regression line indicates a 14% underprediction, but the accuracy in this case is dominated by the offset rather than the

slope. Thus, the average offset, which is about +2.5% high is the best measure of the correlation inaccuracy.

### Forward Flight Performance

The calculation of forward flight performance is particularly important at the maximum flight speed or at the best cruise speed, either of which may be a contractual guarantee. Yeo et al. (Ref. 5) have used CAMRAD II to look at three sets of flight test data on the UH-60: data obtained with the standard blades during the Airloads Program on the UH-60A (Ref. 10), data obtained with the standard blades during a subsequent development program using the UH-60L, and data obtained on a UH-60L with wide chord blades (see Ref. 5 for discussion of data sources). Figure 16 shows power coefficient calculations and measurements for the UH-60A (the data for the airspeed at  $C_W/\sigma = 0.090$  are not included for clarity), and these show the typical form of the power required curve with airspeed and increasing weight. The accuracy of this

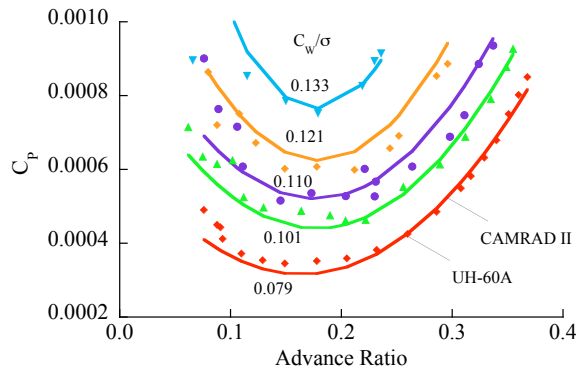


Figure 16. UH-60A  $C_p$  as a function of  $\mu$  for five weight coefficients (airspeed sweeps) compared with CAMRAD II (Ref. 5).

calculation as well as calculations from the UH-60L tests with the standard blade is shown in Fig. 17. For the UH-60A data, there are two independent measurements of power. First, there is the power that is measured at the engine output shafts, which represents the total vehicle power and, second, there is the power based on the main rotor torque measurement. These two sets of measurements are treated as independent data sets, hence Fig. 17 is a combined analysis of three data sets for the power required for a UH-60 with standard blades. There is an overprediction of power of 3.7% and the scatter is high for performance measurements. In particular, some solution points are well away from the 45° line,

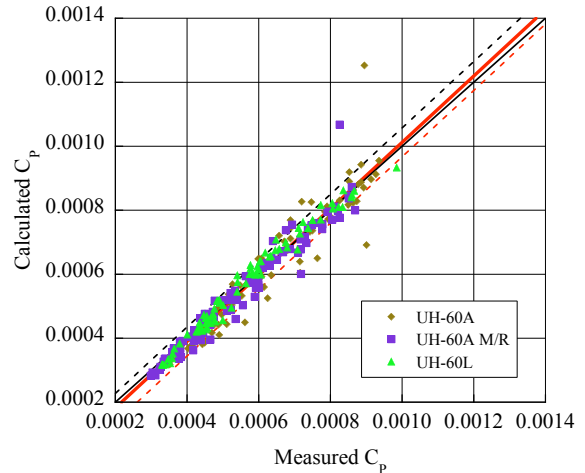


Figure 17. Accuracy of CAMRAD II for the three standard blade data sets (Ref. 5);  $m = 1.037$ ,  $S_e = \pm 3\%$ .

Table 6. Accuracy of CAMRAD II for three standard blade data sets plus wide chord blades (Ref. 5).

Aircraft	Rotor	$m$	$\pm S_e, \%$
UH-60A	std	1.076	4.4
UH-60A (M/R power)	std	1.022	2.9
UH-60L	std	1.024	1.7
UH-60L	wide chord	0.868	2.1

generally those points at either end of the high weight coefficient speed sweeps.

Table 6 shows the individual accuracies for the three sets of data and also includes the accuracy values for the UH-60L with the wide chord blades (these data are proprietary and are not shown in Fig. 17). The total power for the UH-60A tested during the Airloads Program is overpredicted by 7.6% and the scatter is excessive. Power based on the main rotor shaft torque is more accurate and is similar to the total power measurements on the UH-60L. The wide chord blade data are underpredicted by 13.2%, which is an excessive error for performance data for any aircraft. The problems with the accuracy measurements in Table 6 are caused in part by serious temperature calibration errors in the original flight test measurements that have not been resolved (Ref. 11). It may be the case that these flight test measurements are not suitable for the assessment of flight performance accuracy.

A generation ago, Harris et al. (Ref. 1) examined cruise performance predictions for 11 helicopters at various weight coefficients, providing

35 test cases. Of the 35, 18 were within a  $\pm 3\%$  error band and 30 were within  $\pm 6\%$ . No significant improvement in performance prediction has been demonstrated since 1979. If accuracies for forward flight performance are required that are better than Harris et al. demonstrated 35 years ago, then improved measurements will be needed.

### OEI Performance

One-Engine-Inoperative (OEI) performance is evaluated near the minimum power speed, which for a typical helicopter is between an advance ratio of 0.15 and 0.20. Wachspress et al. (Ref. 8), using the CHARM code, have calculated power for a number of rotors near the minimum power speed, including the UH-60A rotor in the 80- by 120-Foot Wind Tunnel at NASA Ames Research Center and the Tilt Rotor Aeroacoustic Model (TRAM) in the German-Dutch Wind Tunnel (DNW).

Figure 18 shows the main rotor power coefficient for the UH-60A rotor for three thrust coefficients over the range of  $0.0 \leq \mu \leq 0.20$ . In this case, the CHARM analysis modeled the wind tunnel walls as panels and the Large Rotor Test Apparatus

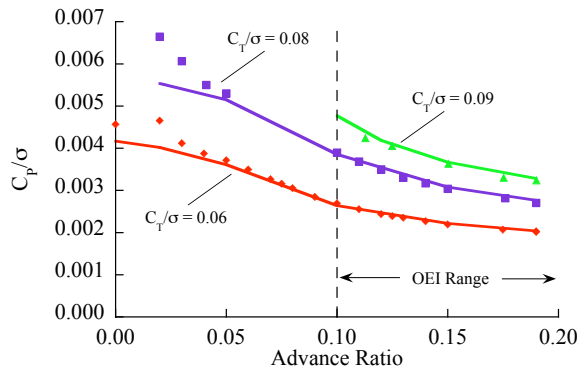


Figure 18. UH-60A  $C_p/\sigma$  as a function of  $\mu$  for three weight coefficients compared with CHARM (Ref. 8).

(LRTA), which supports and powers the rotor, as a body of revolution. The calculations appear quite accurate until deviations in the power prediction are seen at  $\mu \leq 0.04$ , presumably when flow breakdown on the tunnel walls occurs. Of interest for OEI performance is the advance ratio range from 0.10 to 0.20, and the accuracy of the CHARM analysis is assessed over this range in Fig. 19. The CHARM analysis overpredicts the power required by 2.3% and there is very little scatter. The CHARM code was also used to predict the main rotor power without modeling the wind tunnel walls or the LRTA. In this case the power was overpredicted by 13.2%, showing

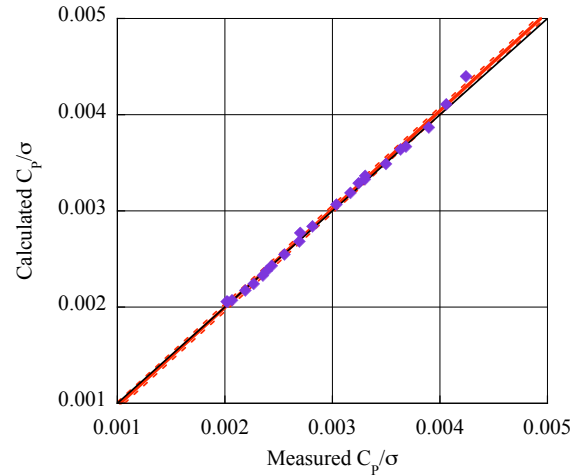


Figure 19. Accuracy of CHARM for three thrust coefficients (Ref. 8) for  $\mu \geq 0.10$ ;  $m = 1.023$ ,  $S_e = \pm 1\%$ .

that wall effects must be correctly modeled for rotors tested at these low speeds.

The CHARM analysis has also been used to predict the power of the TRAM model at  $\mu = 0.15$  in the DNW wind tunnel. In this case, the variables causing variation in the power coefficient are shaft angle of attack and thrust coefficient, as shown in Fig. 20. The calculation in this case is unusual in that

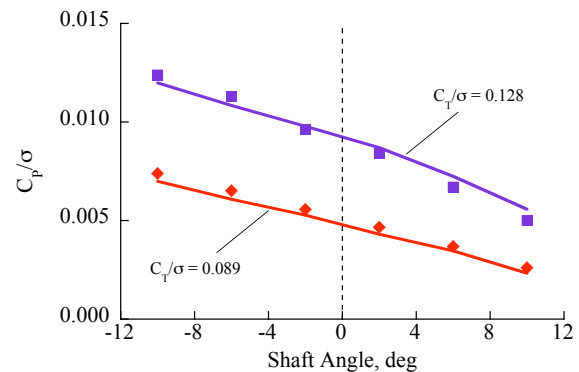


Figure 20. TRAM  $C_p/\sigma$  as a function of shaft angle and thrust coefficient as compared with CHARM (Ref. 8).

it was made blind, that is, the data were not provided to CDI (the developers of CHARM) prior to their making the computation. The accuracy of this calculation is judged in Fig. 21, which shows an underprediction of power by 1.4%, which is comparable to the UH-60A prediction discussed above.

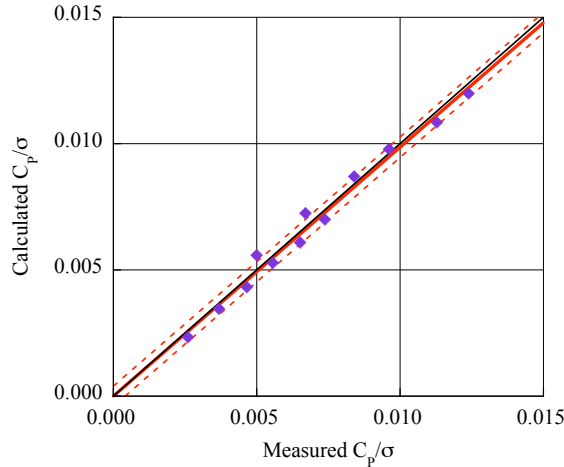


Figure 21. Accuracy of CHARM for TRAM at  $\mu = 0.15$  (Ref. 8);  $m = 0.986$ ,  $S_e = \pm 3\%$ .

Yeo et al. (Ref. 5) have calculated forward flight performance for three UH-60 flight tests as discussed above (see Figs. 16 and 17). These calculations and measurements are examined here for the range  $0.12 \leq \mu \leq 0.22$  to assess the accuracy of predictions for OEI performance using the CAMRAD II analysis. An example comparison of the power prediction over this range is shown in Fig. 22 for the UH-60L with the standard blades at four weight coefficients (airspeed sweeps). For this case, both advance ratio and weight coefficient are the source of variation in the power coefficient. The accuracy of the CAMRAD II analysis is assessed in

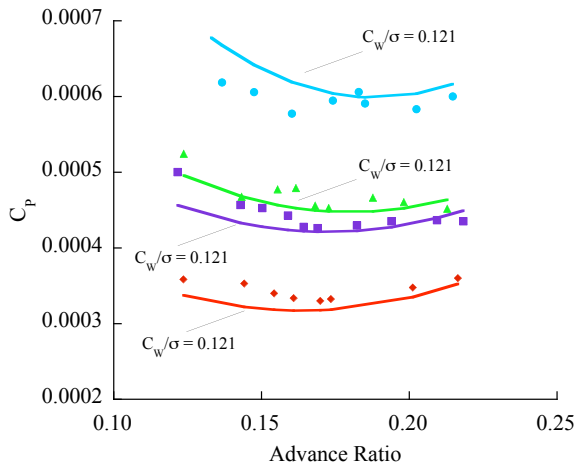


Figure 22. Power coefficient as a function of advance ratio and weight coefficient compared with CAMRAD II for UH-60L with standard blades (Ref. 5).

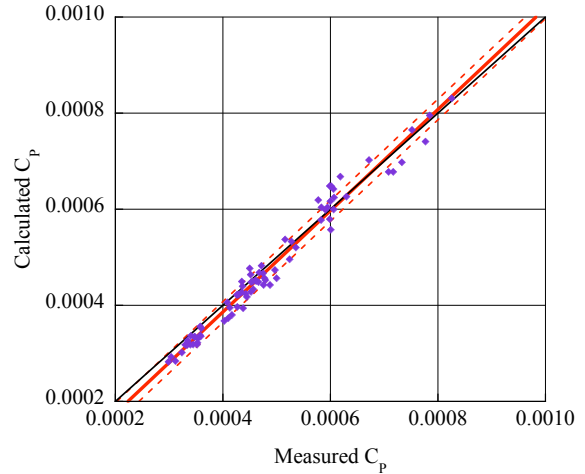


Figure 23. Accuracy of CAMRAD II for OEI performance for three standard-blade data sets (Ref. 5);  $m = 1.054$ ,  $S_e = \pm 2\%$ .

Fig. 23 for the three data sets for the standard blades (again, the wide chord blade data are excluded). There is an overprediction of 5.4%.

Harris et al. (Ref. 1) also examined OEI performance in the Bell Helicopter Textron study of forward flight performance. For the minimum power speed they included data from isolated rotor tests, model rotor tests, and 11 flight tests. Including multiple weight or thrust conditions, this provided 45 cases. Of these, 29 were within a band of  $\pm 3\%$  and 39 were within  $\pm 6\%$ . As noted previously for the hover and forward flight performance, there is no apparent improvement in predictive capability in the last 30 years, although there is less empiricism in present analytical models.

#### Forward Flight Airloads

There are few data sets that include rotor blade airloads. Such experiments require chordwise arrays of pressure transducers, ideally at multiple radial stations. Older experiments, using differential pressure transducers, are able to compute normal force and pitching moment; whereas more recent experiments, employing arrays of absolute pressure transducers, also obtain chord force (but not viscous drag).

Yeo and Johnson (Ref. 12) have looked at five sets of rotor airloads data. Two of these data sets, that of the H-34 and the UH-60A, have measurements at radial stations along the blade span; whereas the other three data sets, flight tests of the research Puma, the SA 349/2, and model tests of the BO 105, have measurements at only a few stations near the blade tip. The correlation effort by Yeo and Johnson selected an outboard radial station from the

five data sets, generally near  $0.90R$ , and then picked two airspeeds: a low speed was selected near  $\mu \sim 0.15$ , where there is strong loading from the vortex wake, and a high speed was selected that was representative of the maximum flight speed. For the H-34, flight-test data were used for the low-speed case, whereas wind tunnel data (same rotor) were used for the high-speed case. There was no high-speed case for the BO 105 wind tunnel tests.

The CAMRAD II calculations were made using two wake models: a rolled-up wake model and a multi-trailer model. Otherwise, analysis options were held constant for all of the cases. Thus, there were 9 test conditions (5 rotors at low speed, 4 rotors at high speed) and two wake models, which resulted in 18 calculations for both normal force,  $M^2c_n$ , and pitching moment,  $M^2c_m$ . An example of the

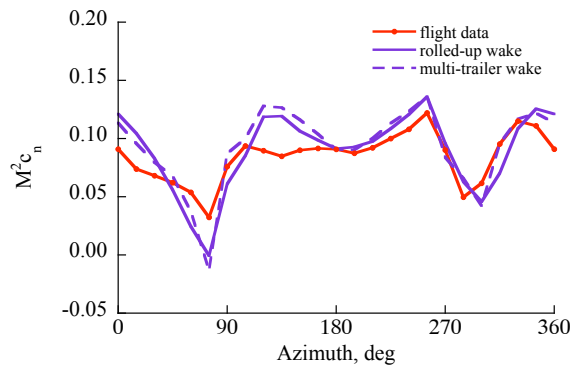


Figure 24. Measured normal force as a function of azimuth on the research Puma compared with CAMRAD II (Ref. 12);  $r/R = 0.92$  and  $\mu = 0.141$ .

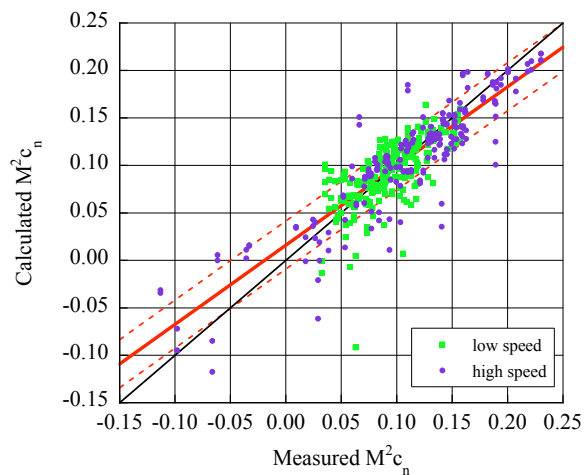


Figure 25. Accuracy of CAMRAD II for combined analysis of 5 rotors at 2 airspeeds (Ref. 12);  $m = 0.834$ ,  $S_e = \pm 10\%$ .

calculation for normal force for the research Puma at low speed is shown in Fig. 24. The time history is sampled every 15 deg. so as to represent the frequency content. The combined analysis of the 18 cases is shown in Fig. 25. There is a general underprediction of about 17% and the scatter is much greater than was seen for the performance calculations. If the low- and high-speed cases are examined separately, the combined results are much the same: at low speed,  $m = 0.814$  and at high speed,  $m = 0.839$ . But if the accuracy of the individual rotors or helicopters is examined separately the results are variable. They range from  $m = 0.138$  for the low-speed BO 105 case to  $m = 1.403$  for the low-speed Puma case. This range of variability makes it difficult to know if the overall slope in Fig. 25 is representative of analysis accuracy.

Similar results are obtained by assessing the accuracy of the blade pitching moments. Figure 26 shows an example for the SA 349/2 where  $\mu = 0.14$  and  $r/R = 0.88$ . This is one of 16 cases (there are no BO 105 data for pitching moment). The poor correlation indicates that the lifting-line model in CAMRAD II does not adequately represent the disk vortex loading for this low-speed case. The combined analysis of the 16 cases for pitching moment is shown in Fig. 27. The underprediction for pitching moment is about 25% and the scatter is increased over that seen for normal force. In the normal force case, little difference was seen in the computed slope for the separate analyses of the low- and high-speed cases. But for pitching moment at low speed,  $m = 0.828$  and  $S_e = \pm 16\%$ , whereas at high speed,  $m = 0.727$  and  $S_e = \pm 31\%$ . Analysis of the accuracy of the individual rotors shows considerable variation, as was seen for normal force. The slopes vary from  $-0.040$  for the SA 349/2 at low speed (see Fig. 26) to  $1.029$  for the H-34 at high speed.

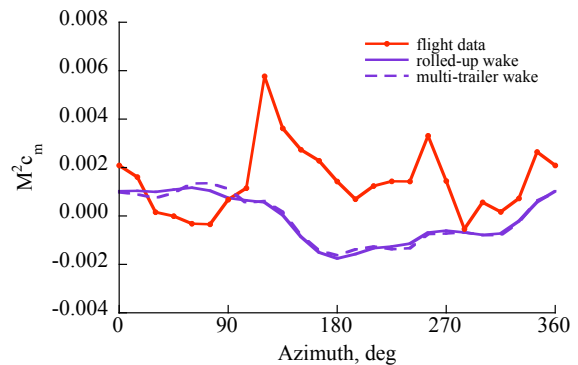


Figure 26. Measured pitching moment as a function of azimuth on the SA 349/2 compared with CAMRAD II (Ref. 12);  $r/R = 0.88$  and  $\mu = 0.14$ .

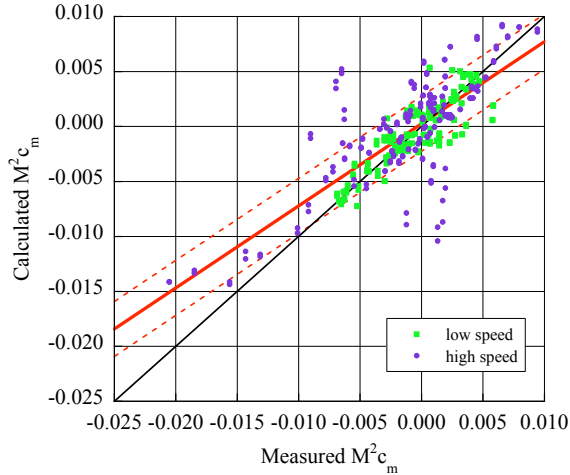


Figure 27. Accuracy of CAMRAD II for combined analysis of 4 rotors at 2 airspeeds (Ref. 12);  $m = 0.747$ ,  $S_e = \pm 25\%$ .

#### Blade Structural Loads in Forward Flight

The correct calculation of blade structural loads, that is, the flap bending, chord bending, and torsion moments, is important for fatigue and vibration. Yeo and Johnson (Ref. 5) have used CAMRAD II to compare with the structural loads from the same five experiments that were examined for their airloads in the previous section. For this effort they selected loads measured roughly at the midspan on the blade. Again, the same two airspeeds were selected, one near  $\mu \sim 0.15$ , where there is strong loading from the vortex wake, and one at high speed. For the low-speed case, flight test data was used for the H-34, whereas for the high-speed case, wind tunnel data were used (same rotor, different tests). There was no high-speed case for the BO 105 wind tunnel tests.

The CAMRAD II calculations were made using two wake models: a rolled-up wake model and a multi-trailer model. Otherwise, analysis options were held constant for all of the cases. Thus, there were 9 test conditions (5 rotors at low speed, 4 rotors at high speed) and two wake models, which resulted in 18 calculations each for the flap bending, chord bending, and torsion moments.

An example of flap bending moment on the research Puma at high speed is shown in Fig. 28. For the comparisons of structural loads, the mean values of the measurements and calculations have been removed. As with the blade airloads, the variation in the regression analysis is provided by sampling the time histories every 15 deg. The combined analysis of the 18 sets of comparison are shown in Fig. 29. Based on this combined analysis there is an underprediction of 27%. The predictive accuracy in

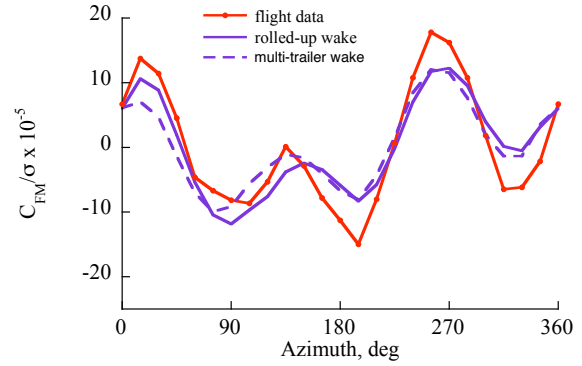


Figure 28. Nondimensional flap bending moment as a function of azimuth on the Puma compared with CAMRAD II (Ref. 5);  $r/R = 0.46$  and  $\mu = 0.362$ .

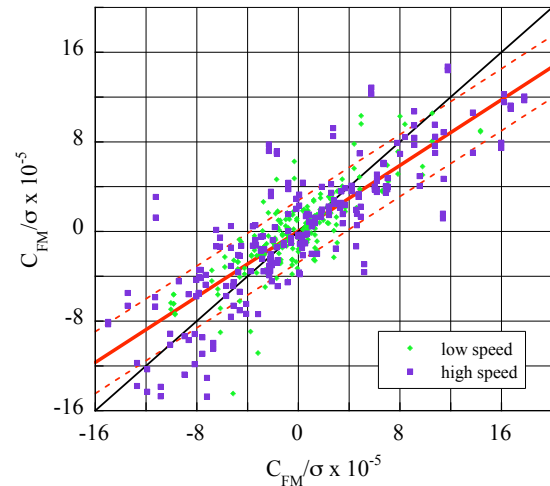


Figure 29. Accuracy of CAMRAD II for combined analysis of midspan flap bending moment for 5 rotors at 2 airspeeds (Ref. 5);  $m = 0.733$ ,  $S_e = \pm 14\%$ .

this case is less than was observed in the previous normal force comparisons. This is not surprising since the blade normal forces largely determine the flap bending moments. As with the previous normal force assessment, there is little difference between the low- and high-speed cases for flap bending moment,  $m = 0.761$  at low speed and  $m = 0.722$  high speed. Also, as seen for the airloads comparisons, there is a wide variation in the slope values for the 18 cases, the range at low speed extends from a slope of 0.372 for the BO 105 to 1.080 for the UH-60A.

An example of the CAMRAD II prediction of chord bending moment is shown in Fig. 30 for the SA 349/2 at high speed. The combined analysis of the 18 cases for chord bending is shown in Fig. 31. The combined accuracy in this case is poor. The underprediction of 73% is so large as to make the calculations largely untrustworthy. There are

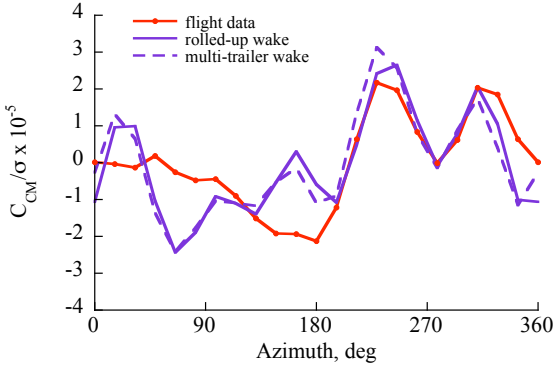


Figure 30. Nondimensional chord bending moment as a function of azimuth on the SA 349/2 compared with CAMRAD II (Ref. 5);  $r/R = 0.54$  and  $\mu = 0.361$ .

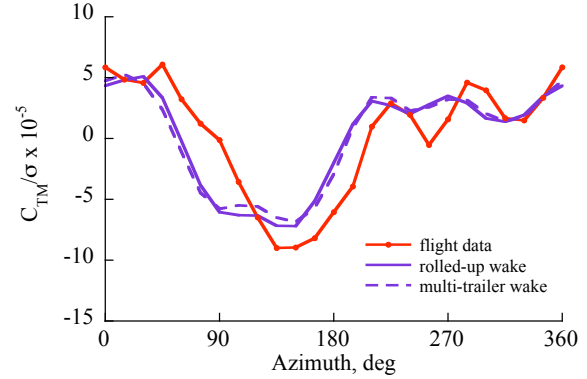


Figure 32. Nondimensional torsion moment as a function of azimuth for the UH-60A compared with CAMRAD II (Ref. 5);  $r/R = 0.30$  and  $\mu = 0.368$ .

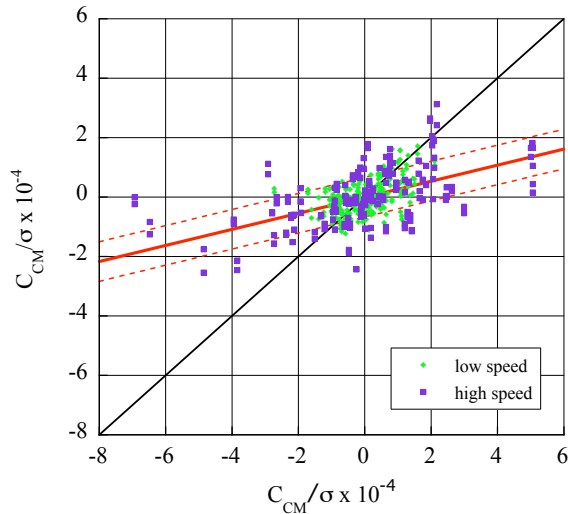


Figure 31. Accuracy of CAMRAD II for combined analysis of midspan chord bending moment for 5 rotors at 2 airspeeds (Ref. 5);  $m = 0.271$ ,  $S_e = \pm 11\%$ .

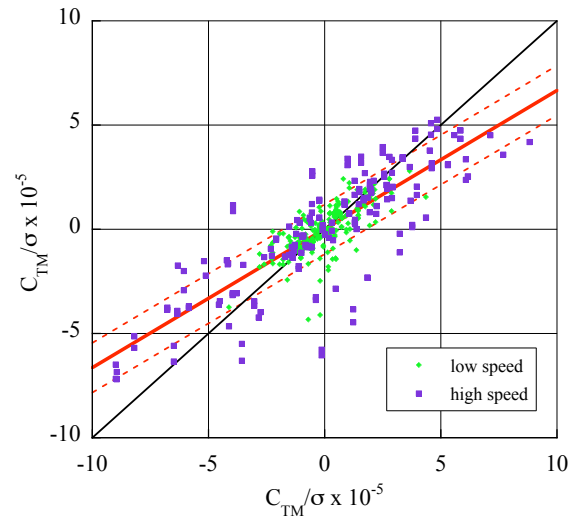


Figure 33. Accuracy of CAMRAD II for combined analysis of midspan torsion moment for 5 rotors at 2 airspeeds (Ref. 5);  $m = 0.665$ ,  $S_e = \pm 12\%$ .

differences between the airspeed regimes, with the a 64% underprediction at low speed and 75% at high speed. The variation between individual cases ranges from  $-86\%$  for the Puma to  $-25\%$  for the SA 349/2 (both at high speed).

It is expected that the chord bending calculation will be influenced by the rotor's lead-lag damper, particularly at inboard locations. The H-34, research Puma, and UH-60A all use hydraulic dampers that have strong nonlinearities. The SA 349/2 uses an elastomeric damper with weaker nonlinearities. The BO 105 does not have a damper, but there is probably some friction damping in the blade root attachment. But the differences in predictive accuracy for chord bending for these five rotors bear no obvious relationship to the damper type.

An example of CAMRAD II calculation of torsion moment for the UH-60A is shown in Fig. 32. The combined analysis of the 18 cases for torsion moment is shown in Fig. 33. There is an underprediction of about 33% for these cases, which is comparable to the underprediction that was seen for the outboard pitching moments (see Fig. 27). If the combined analysis is done for the two airspeed regimes separately, there is little difference in the slopes:  $m = 0.678$  at low speed and  $m = 0.663$  at high speed. But as before, there is considerable variation between individual cases, ranging from  $m = 0.526$  for the Puma at high speed to  $m = 0.879$  for the BO 105 at low speed.

The approach to evaluating predictive accuracy for the blade moments employed here uses the blade azimuth angle (time history) to provide a

range of values for assessment. For the design engineer who is interested in fatigue damage, small differences in time histories are not of concern. Rather, it is the peak-to-peak loading that occurs over a wide range of conditions that is most meaningful. Using the Yeo and Johnson (Ref. 5) calculations and data it is possible to compute the peak-to-peak loads for these same cases and assess the predictive accuracy based only on these peak-to-peak loads, as shown for the flap bending moments in Fig. 34. A

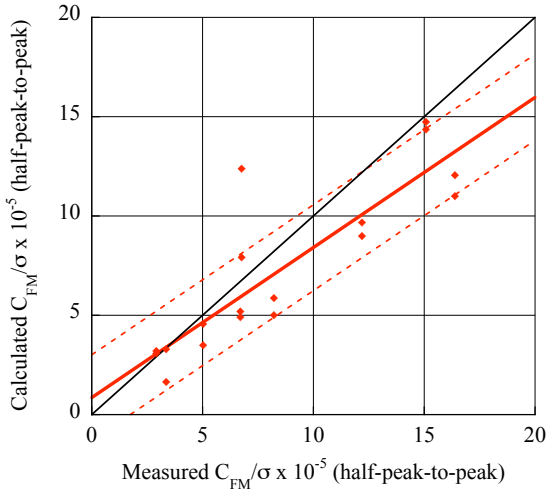


Figure 34. Accuracy of CAMRAD II for half peak-to-peak flap bending moments for 5 rotors and 2 airspeeds (Ref. 5);  $m = 0.756$ ,  $S_e = \pm 11\%$ .

comparison of the slopes and the standard errors for the flap and chord bending, and torsion moments using the time histories (referred to here as the azimuth approach) is compared with that obtained using the peak-to-peak data in Table 7. The slopes for flap bending and torsion moment accuracy are much the same for both approaches, although the scatter as indicated by  $S_e$  is less for the peak-to-peak assessment. The accuracy of the chord bending moment peak-to-peak prediction is improved as compared to the azimuth approach, but remains inaccurate.

Table 7. Comparison of slope and standard error of estimate for azimuth and peak-to-peak approaches.

	Flap		Chord		Torsion	
	$m$	$S_e$	$m$	$S_e$	$m$	$S_e$
azim.	0.733	14%	0.271	11 %	0.665	12%
p-to-p	0.756	11%	0.409	9%	0.674	7%

### Maneuver Loads

Maneuver loads size many of the blade components, both in the rotating and fixed systems. Compared to a maximum airspeed level flight condition, blade loads are often doubled during severe maneuvers and the control loads may increase by a factor of 2.5 or 3.0 (Ref. 13). Analytical methods are not considered reliable for these calculations so currently these design loads are determined from flight test databases. Recent developments, however, offer optimism that some improvement can be achieved, even with comprehensive analyses.

Recently, Bhagwat et al. (Ref. 14) have studied the maneuver loads problem using a coupled approach employing RCAS (Ref. 15) for the Computational Structural Dynamics (CSD) side and OVERFLOW-2 (Ref. 16) for the Computational Fluid Dynamics (CFD) side. They focused on the UTTAS maneuver for the UH-60A where the aircraft enters the maneuver at its maximum level flight speed, pulls up to achieve a 1.75-g load factor, and attempts to maintain that load factor for 3 seconds. This maneuver, in terms of loading, is one of the most severe encountered in the U.S. Army/NASA Airloads Program (Ref. 13).

Figure 35 shows the half peak-to-peak pitch-link loads during the UTTAS maneuver and compares these with RCAS alone and the coupled RCAS/OVERFLOW-2. The half peak-to-peak loads predicted by RCAS are shown in Fig. 36, which shows a 40% underprediction. The maneuver loads in this case are dominated by dynamic stall (Ref. 17)

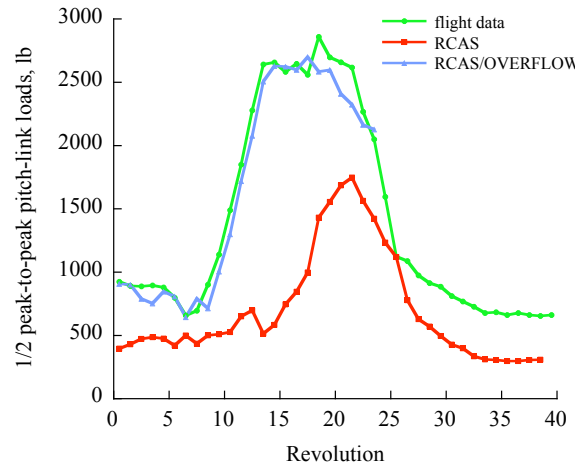


Figure 35. Half peak-to-peak pitch-link loads during UTTAS maneuver on UH-60A compared to RCAS/OVERFLOW-2 coupled solution and RCAS alone (Ref. 14).

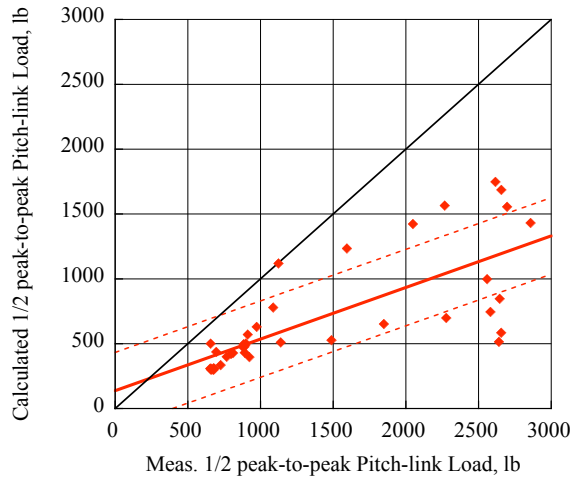


Figure 36. Accuracy of RCAS prediction for pitch-link loads during UTTAS maneuver (Ref. 14);  $m = 0.398, S_e = \pm 10\%$ .

and the poor prediction of pitch-link loads under these conditions is typical of comprehensive analyses. But the prediction of the loads using the CSD/CFD analysis is quite good. Table 8 shows the slopes and standard error of estimate for three load components during the UTTAS maneuver and compares the RCAS and the CSD/CFD predictions. Both approaches show good results for the flap bending moments, being within 5 to 8% of the measurements. RCAS compares very well with the chord bending moments, but the CSD/CFD underpredicts these moments. The coupled CSD/CFD calculation for the pitch-link loads is very good, showing this coupled approach is able to capture most of the features of the dynamic stall loading.

#### Fixed-System Loads

The measurement of the vibratory loads in the fixed system is extraordinarily difficult (as is the calculation). Gabel et al. (Ref. 18) used multiple approaches to measure vibratory loads in both the rotating- and fixed-systems, and their study illustrates many of the experimental difficulties. Sikorsky Aircraft tested a five-bladed bearingless rotor, the

SBMR, in the 40- by 80-Foot Wind Tunnel in 1992. The 5/rev loads were measured in the fixed system, and three different comprehensive analyses were used to predict these fixed-system loads (Ref. 19). The fixed-system measurements were obtained with a dynamically calibrated balance and dynamic corrections were applied to the measured pitch-link loads as well. There were five components of the balance loads (all the forces and moments except torque) and the published results have unfortunately been normalized by an arbitrary factor. Three Sikorsky Aircraft analyses were compared with the measurement: two analyses developed by the company, KTRAN and RDYNE; and UMARC/S, a proprietary version of the University of Maryland's comprehensive analysis code. Figure 37 provides an example of the measurements of the 5/rev vertical force for the SBMR as a function of airspeed and includes the predictions of the three codes, which show widely differing predictions. A combined analysis of all load components and calculations is shown in Fig. 38. Such a combined analysis as shown here has serious limitations. For example, it is difficult to equate the 5/rev drag force with the 5/rev rolling moment, so the five load components are apples and oranges and different kinds of fruit. Moreover, because the loads have been normalized, the grouping for combined analysis is even less satisfactory. A more appropriate comparison is to look at each individual case as is shown in Table 9. There are only a few situations where a component of the balance load is predicted within  $\pm 25\%$ ; in most cases, the errors are much larger. But the scatter as measured by the standard error of estimate is good in most cases. Even for the most accurate code, UMARC/S, the predictions are poor.

#### Wake and Fuselage Interactions

The rotor wake will cause loading on the fuselage and the fuselage will change the inflow at the rotor. These interaction effects can be quite pronounced when they affect empennage loading or cause boundary layer separation. The CHARM code can represent a helicopter body using a panel method.

Table 8. Comparison of RCAS and coupled RCAS/OVERFLOW-2 predictive capabilities for UTTAS maneuver loads.

	Flap (0.50R)		Chord (0.50R)		Pitch Link	
	$m$	$S_e$	$m$	$S_e$	$m$	$S_e$
RCAS	1.078	9%	1.012	18%	0.398	10%
RCAS/OVERFLOW-2	0.949	10%	0.586	13%	0.963	4%

Table 9. Comparison of slope and standard error of estimate for five components of balance loads using three Sikorsky Aircraft analyses.

BALANCE LOAD	KTRAN		UMARC/S		RDYNE	
	$m$	$S_e$	$m$	$S_e$	$m$	$S_e$
drag force	0.331	2%	0.678	20%	0.614	7%
side force	0.197	3%	1.557	8%	0.306	8%
pitch moment	0.548	14%	1.243	9%	1.549	28%
roll moment	0.073	10%	0.474	13%	-0.210	10%
vertical force	-0.042	11%	0.872	6%	1.049	5%

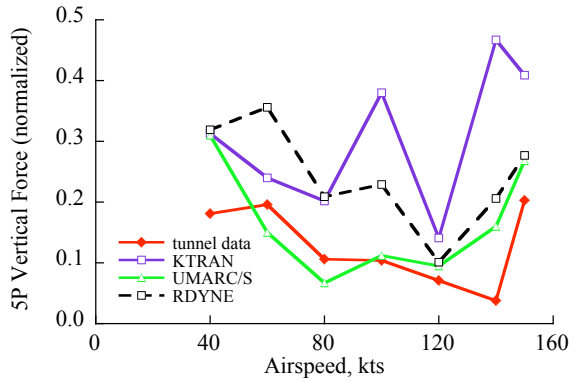


Figure 37. Normalized 5/rev balance vertical force as a function of airspeed compared with three calculations (Ref. 19).

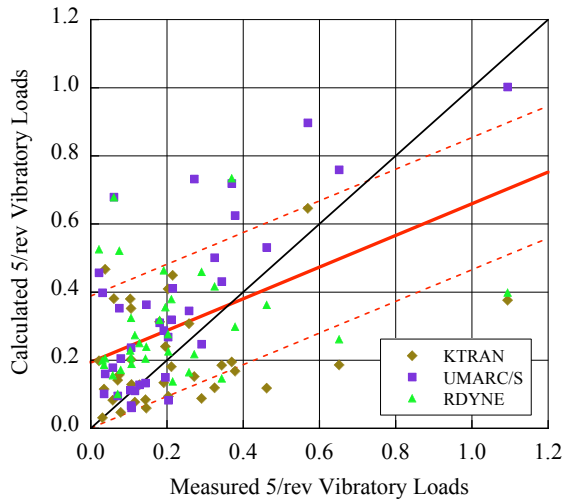


Figure 38. Accuracy of Sikorsky analyses for the prediction of 5/rev balance loads (Ref. 19);  $m = 0.465$ ,  $S_e = \pm 16\%$ .

Wachspress et al. (Ref. 20) have compared the CHARM code with experimental data from a test of a model Dauphin rotor and fuselage. Figure 39 provides an example of the calculated and measured unsteady pressure at a centerline location on the

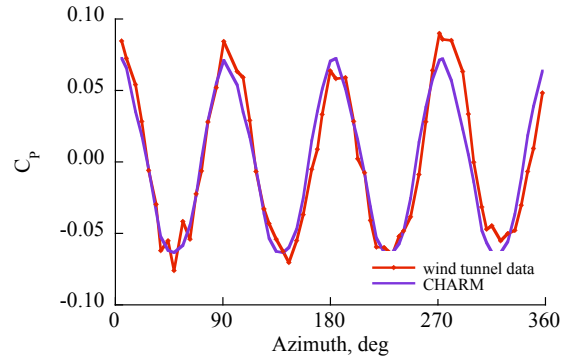


Figure 39. Unsteady pressures on Dauphin fuselage from combined rotor and fuselage test, comparing CHARM calculations and measurements (Ref. 20).

forward part of the fuselage. To assess the calculation, 15 pressure taps were used for the comparison: 5 were on the fuselage centerline and 10 were on the fuselage sides at two longitudinal locations. Variation in the analysis variables was provided by sampling at various azimuths (as seen in Fig. 39) and using multiple pressure tap locations. Figure 40 shows the predictive accuracy of the CHARM analysis for the unsteady pressure prediction. The combined accuracy is quite good, with a 7% underprediction. The accuracy at individual stations ranged from  $m = 0.677$  at a centerline location immediately behind the rotor hub to  $m = 1.080$  at a centerline location on the empennage. Most of the individual slopes were close to  $m = 0.9$ .

#### Active Controls

Tests of model- and full-scale rotors in recent decades have demonstrated a number of active control approaches that can reduce vibration and noise, including higher-harmonic control (HHC) and individual blade control (IBC). In each of these demonstrations, some form of controller was used that measured vibratory loads and calculated the active control input that would provide a reduction.

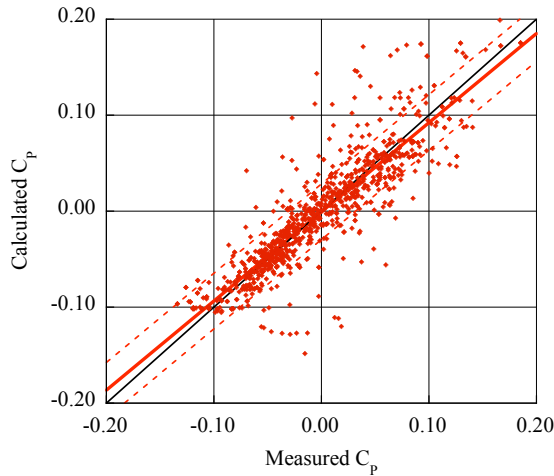


Figure 40. Accuracy of CHARM predicted unsteady pressures for 15 locations on Dauphin fuselage (Ref. 20);  $m = 0.929$ ,  $S_e = \pm 15\%$ .

But few attempts have been made to correlate with these control inputs.

A full-scale BO 105 rotor with an IBC control system was tested in the 40- by 80-Foot Wind Tunnel in two phases in 1993 and 1994 (Ref. 21). The active control in this test was a hydraulically actuated pitch link between the rotating swashplate and the blade root. Torok (Ref. 22) used a Sikorsky version of the UMARC code to predict the effects on 4/rev hub loads with changes in the pitch link 2/rev and 3/rev input phase angles. Because there was no calibrated dynamic balance, Torok computed the percent change in the loads rather than the actual loads themselves. Figure 41 shows the measured change in 4/rev hub shear with the variation in phase of the 2/rev input and compares this to the UMARC/S predictions. A combined analysis of the predicted changes in 4/rev hub shears, moments, and

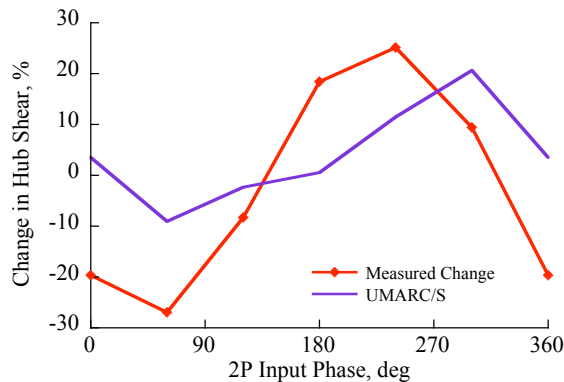


Figure 41. Change in 4/rev hub shear as a function of IBC 2/rev input phase for BO 105 in the wind tunnel; comparison of measurements and UMARC (Ref. 22).

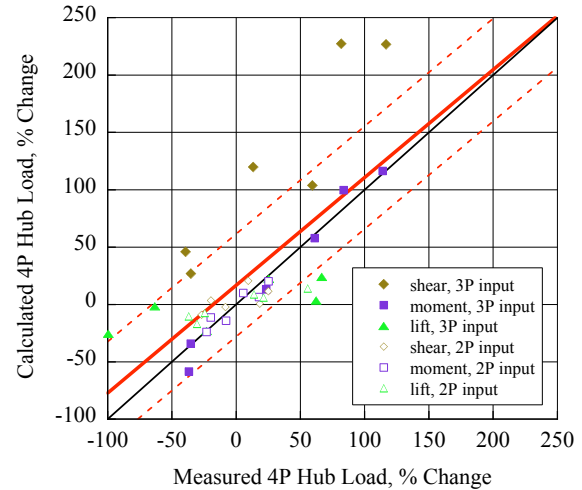


Figure 42. Accuracy of UMARC/S prediction of 4/rev hub load change with variable 2/rev and 3/rev IBC inputs (Ref. 22);  $m = 0.939$ ,  $S_e = \pm 18\%$ .

lift is shown in Fig. 42. Variation in the correlation variables is provided by the 2/rev and 3/rev input phase angles of the active pitch link, and the three components of hub loads. The predictive accuracy in this case, judged by the slope 0.939 for the combined analysis, is very good. But when the individual components are examined, as shown in Table 10, it is observed that most of the calculations are quite poor, only the 4/rev hub moment change to 3/rev phase inputs is within  $\pm 20\%$  of the measurements. This example shows that caution needs to be used in combining data sets for the quantitative approach presented here. Combining cases may be effective in some situations but misleading in others.

Table 10. UMARC/S predictive accuracy for changes in 4/rev hub loads with 2/rev and 3/rev input phase variation for full-scale BO 105 with IBC (Ref. 22)

Hub Component	Input	$m$
Shear	2/rev	0.310
Moment	2/rev	0.797
Lift	2/rev	0.318
Shear	3/rev	1.251
Moment	3/rev	1.126
Lift	3/rev	0.240

Kottapalli (Ref. 23) has examined data for a UH-60A rotor tested in the 80- by 120-Foot Wind Tunnel in 2001 with an IBC system installed. He used CAMRAD II to compare with the test data. As the balance was uncalibrated, Kottapalli compared

calculations and measurements for the blade loads that cause the 4/rev fixed frame vibrations, that is, 3/rev and 5/rev chord bending moments, and 4/rev flap bending moments. An example of the measured and calculated 3/rev chord bending moment responses to a 3/rev IBC input over a range of phase angles is shown in Fig. 43. In this particular example the agreement appears fairly good. A combined analysis of the 3/rev chord bending moment response at three radial stations is shown in Fig. 44. The

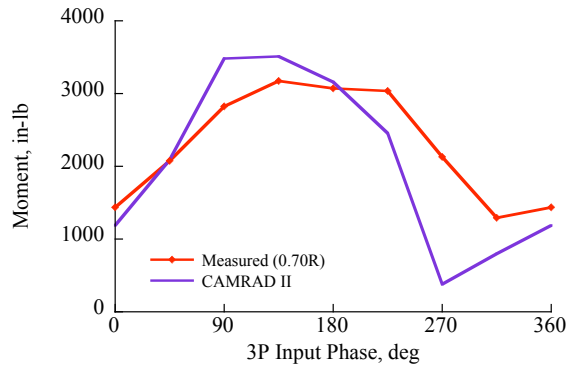


Figure 43. Change in measured 3/rev chord bending moment of UH-60A with IBC, compared with CAMRAD II (Ref. 23).

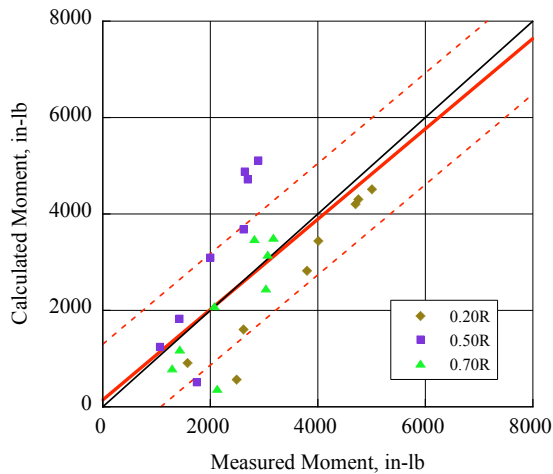


Figure 44. Accuracy of CAMRAD II prediction of 3/rev chord bending moments with variable 3/rev IBC inputs (Ref. 23);  $m = 0.937$ ,  $S_e = \pm 14\%$ .

accuracy of the combined analysis is quite good,  $m = 0.937$ . But as in the previous case of the BO 105 with IBC inputs, the combining of these three radial stations obscures the poor correlation that was obtained for the individual cases, as shown in the first row of Table 11. Again, as was the case for the BO 105 correlation, the use of a combined analysis can be misleading. In the present case, the

Table 11. CAMRAD II predictive accuracy for blade bending moment response at 3 radial stations for UH-60A with IBC (Ref. 23).

Bending Moment	Resp.	$m$		
		0.20R	0.50R	0.70R
Chord	3/rev	1.219	2.349	1.365
Chord	5/rev	-0.624	-0.773	-0.424
Flap	4/rev	0.480	1.729	0.279

combining of the chord bending moment response at three radial stations seems entirely appropriate since these independent measurements should be related through the actual blade modes. But despite this argument, which seems reasonable, the combined analysis does not appear successful in this case. Table 11 also shows the slope of the regression fit for the 5/rev chord bending and 4/rev flap bending moments. There is wide variation in these values and the ability to predict the response of blade bending moments to active controls is deficient.

#### Aeromechanical/Aeroelastic Stability

There exists an extensive literature on aeroelastic and aeromechanical stability dating back to the earliest rotorcraft flight tests. For current rotorcraft designs, the major stability problems are those dealing with tiltrotor whirl stability and rotorcraft air and ground resonance.

Bell Helicopter Textron has used their stability code, ASAP, to predict whirl stability boundaries for two wing designs tested at model scale in NASA Langley's Transonic Dynamics Tunnel (Ref. 24). Figure 45 shows the stability boundaries for the two wing designs. For each rotor

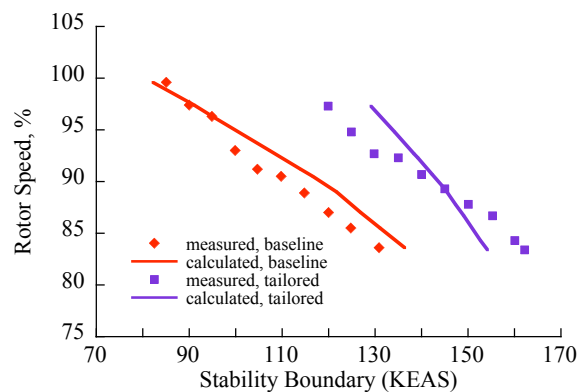


Figure 45. Whirl flutter stability boundaries for two wing designs as tested in the Transonic Dynamics Tunnel compared with Bell Helicopter Textron's ASAP analysis (Ref. 24).

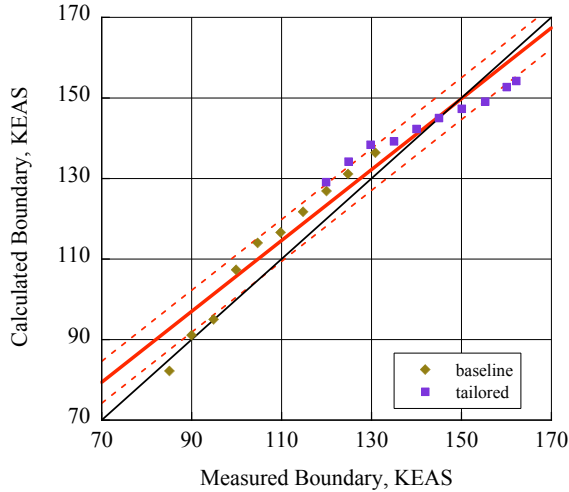


Figure 46. Accuracy of ASAP prediction of whirl flutter stability boundaries for two wing designs (Ref. 24);  $m = 0.880$ ,  $S_e = \pm 3\%$ .

speed, the boundary (in knots equivalent airspeed) where the damping becomes neutral is shown. The linear regression for these boundary points, where rotor speed is the source of the variation in the correlation variables, is shown in Fig. 46. The stability boundary is underpredicted by 12%. The scatter as indicated by the standard error of estimate is low.

Peterson and Johnson (Ref. 25) have compared the stability predictions of the comprehensive code CAMRAD/JA (a predecessor to CAMRAD II) with measurements obtained in hover (in the 40- by 80-Foot Wind Tunnel) for a full-scale BO 105 rotor. Rotor thrust provided the variation in the correlation variables. The damping as a function of thrust is shown in Fig. 47. The linear regression analysis of these data is shown in Fig. 48. The damping is underpredicted, although the scatter in the

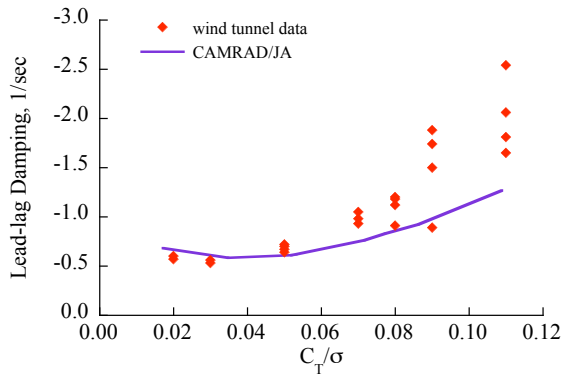


Figure 47. Lead-lag damping of BO 105 in hover in 40- by 80-Foot Wind Tunnel, compared with CAMRAD II (Ref. 25).

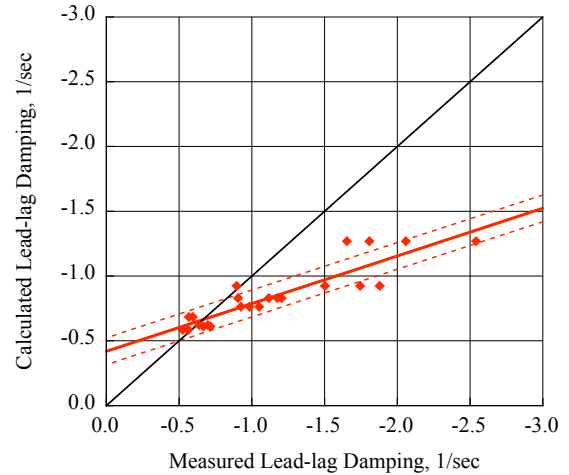


Figure 48. Accuracy of CAMRAD II prediction of BO 105 lead-lag damping (Ref. 25);  $m = 0.368$ ,  $S_e = \pm 3\%$

results is low. To some extent, this is a typical result for aeromechanical stability testing since the accuracy of damping measurements is degraded at higher damping values. But even if half of the points in Fig. 47 were removed, those with the largest damping, the prediction would still be poor.

#### Ice Accretion

Britton (Ref. 26) has examined the torque rise in icing conditions on a model rotor in the NASA Glenn Icing Research Tunnel (IRT). As shown in Fig. 49, there is initially a fairly rapid increase in the torque as ice is deposited, but the rise levels out after ice starts to shed from the outer portions of the blades. Empirical methods for performance degradation and ice shedding generally show good agreement with experimental data taken on model rotors. The correlation method in Fig. 49 (Ref. 27) is able to accurately match this torque rise;  $m = 0.995$ ,

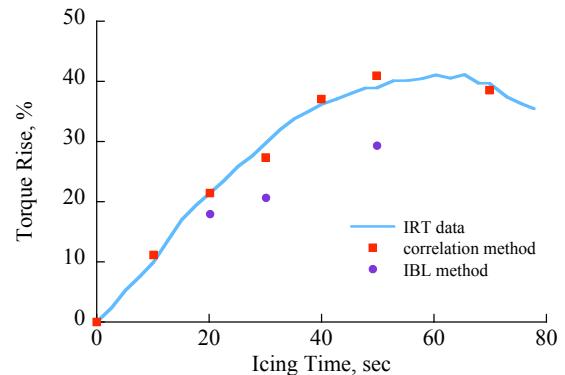


Figure 49. Torque rise on model rotor in NASA Glenn Icing Research Tunnel (Ref. 26).

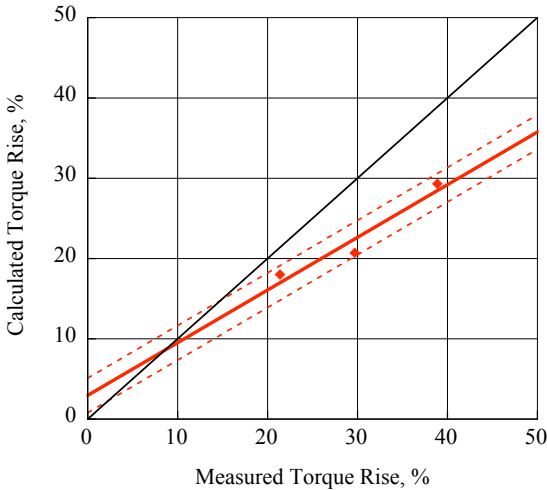


Figure 50. Accuracy of IBL model for prediction of torque rise on model rotor in NASA Glenn Icing Research Tunnel (Ref. 26);  $m = 0.656$ ,  $S_e = \pm 4\%$ .

$S_e = \pm 3\%$ . But because of the nature of empirical methods it is unclear whether these methods can be accurately and consistently applied to full-scale configurations. An analytical approach by Britton (Ref. 26), combines the Boeing B65 performance code, a modified version of the LEWICE ice accretion code, an empirical routine to predict natural shedding, and an interactive boundary layer (IBL) routine to determine the lift and drag characteristics. The predictive accuracy of this combined codes is evaluated in Fig. 50. This method, although closer to a first-principles analysis than the correlation method, underpredicts the torque rise.

### Concluding Remarks

A technique to quantitatively assess the predictive capability of aeromechanics methods has been described in this paper. The method considers some appropriate measurement to be the primary independent variable and the calculated result as the dependent variable. The linear regression of these variables is computed and the slope of the regression line is considered a measure of accuracy. Perfect agreement would provide a slope of 1; values greater than 1 represent overprediction whereas values less than 1 are underprediction. The standard error of estimate of the linear regression is a measure of scatter or dispersion, and in some cases may provide a better assessment of accuracy than the regression line slope. In a few cases, the offset of the linear regression provides a better indicator of error. For the technique to be useful in comparing computation and measurement, however, there must be significant variation in the dependent variables. The method is

based on simple statistical methods that are readily available in any spreadsheet program or with any statistical software package.

Because the method is based on linear regression of data representing measurement and calculation, it is simple to apply over a wide range of problems as has been shown here. The correlation variables may not be strictly stochastic in all cases, and the use of simple statistical tools, such as linear regression, in this sense are a convenience.

But the problem of statistical independence looms large in combining data sets, as has been done here in multiple examples. It is considered a strength of the approach that it is possible to combine multiple cases, for example, two or three independent flight tests for performance or four or five separate tests for blade airloads. But each of these separate tests may have their own problems with differing error sources, and by combining the analysis of these independent tests, these differing error sources may be obscured.

The major emphasis in this paper has been on the accuracy of computation based on the slope of the resulting regression line. The slope is an absolute measurement and is particularly useful. But when expressing the standard error of the estimate or the offset, it is necessary to select a reference condition. In this paper the reference has been the figure's ordinate scale, but this is arbitrary.

A useful feature of the present approach when applied over a broad range of problems is that it describes a hierarchy of predictive accuracy. At the upper end of the hierarchy, such as for hover or forward flight performance, accuracies of the order of  $\pm 1$  or  $\pm 2\%$  appear essential and scatter of  $S_e > 3$  or  $4\%$  seems excessive. Lower down on the hierarchy, errors of  $\pm 10\%$  in the prediction of fuselage unsteady pressures may be acceptable, and the best that can be presently done with blade airloads is of the order of  $\pm 20\%$  or  $\pm 30\%$ . Similarly, stability predictions within  $\pm 10\%$  or  $\pm 20\%$  may be acceptable. Blade structural loads are more difficult to predict, vibratory loads are worse, and the prediction of fixed-system vibration is so difficult that it seems pointless to even call out a particular number.

The hierarchy of these problems may be useful in the sense that it can identify where further research is most needed. Performance predictions for conventional rotors are sufficiently accurate that additional progress can only be obtained with more accurate measurements than are currently obtained. On the other end of the hierarchy, it appears clear that increases in both analysis and measurement accuracy are required.

It has been shown here that phase errors in time histories tend to have significant effects upon

both the slope and the standard error. When the phase errors are significant, then the use of the statistical measures used here become unreliable. This is possibly a benefit rather than a detriment of the approach, since phase errors are a clear indicator that the physics of the problem have not been captured.

The simplicity of the method shown here may have some utility in applications where extensive calculations are being made against many data sets, as sometimes occurs for CFD calculations. Rather than using extensive data visualization to compare calculation and data, the use of the present method may provide a guide as to where major problems in correlation are occurring and the analyst can then focus on these areas.

In addition, as experience is gained in applying this quantitative approach to additional data sets, it may be possible to develop benchmarks concerning the state of the art. If multiple cases in one topic area achieve a similar result, then it will be possible to establish a benchmark for the accuracy of the methods used. This benchmark can then guide further work, whether it be on the analytical or on the measurement side.

#### References Cited

1. Harris, F. D., J. D. Kocurek, T. T. McLarty and T. J. Trept, Jr., "Helicopter Performance Methodology at Bell Helicopter Textron," Amer. Hel. Soc. 35th Annual National Forum, Washington, D.C., 1979.
2. Kocurek, J. D., L. F. Berkowitz and F. D. Harris, "Hover Performance Methodology at Bell Helicopter Textron," Amer. Hel. Soc. 36th Annual Forum, Washington, D.C., 1980.
3. Bousman, W. G. and Thomas H. Maier, "An Investigation of Helicopter Rotor Blade Flap Vibratory Loads," Amer. Hel. Soc. 48th Annual Forum, Washington, D.C. 1992.
4. Bennett, R. L., "Panel 1: Prediction of Rotor and Control System Loads," *Rotorcraft Dynamics*, NASA SP-352, 1974, p. 306.
5. Yeo, H., W. G. Bousman and W. Johnson, "Performance Analysis of a Utility Helicopter with Standard and Advanced Rotors," *J. Amer. Hel. Soc.*, Vol. 49, (3), 2004, pp. 250-270.
6. Yeo, H. and W. Johnson, "Comparison of Rotor Structural Loads Calculated Using Comprehensive Analysis," 31st Eur. Rotorcraft Forum, Florence, Italy, 2005.
7. Felker, F. F., T. R. Quackenbush, D. B. Bliss and J. S. Light. 1988. "Comparison of Predicted and Measured Rotor Performance in Hover Using a New Free Wake Analysis." Amer. Hel. Soc. 44th Annual Forum, Washington, D.C., 1988.
8. Wachspress, D. A., T. R. Quackenbush and A. H. Boschitsch, "First-Principles Free-Vortex Wake Analysis for Helicopters and Tiltrotors," Amer. Hel. Soc. 59th Annual Forum, Phoenix, AZ, 2003.
9. Harris, F. D., "AHIP: the OH-58D from Conception to Production," Amer. Hel. Soc. 42nd Annual Forum, Washington. D.C., 1986 (full-length version)
10. Kufeld, R. M., D. L. Balough, J. L. Cross, K. F. Studebaker, C. D. Jennison and W. G. Bousman, "Flight Testing of the UH-60A Airloads Aircraft." Amer. Hel. Soc. 50th Annual Forum, Washington, D.C., 1994.
11. Bousman, W. G., "Power Measurement Errors on a Utility Aircraft." Amer. Hel. Soc. Aerodynamics, Acoustics, and Test and Evaluation Technical Specialists Meeting, San Francisco, CA, 2002.
12. Yeo, H. and W. Johnson. "Assessment of Comprehensive Analysis Calculation of Airloads on Helicopter Rotors," *J. Aircraft* 42:1218-1228, 2005.
13. Kufeld, R. M., and W. G. Bousman, "High Load Conditions Measured on a UH-60A in Maneuvering Flight," *J. Amer. Hel. Soc.* Vol. 43, (3), 1998, pp. 202-211.
14. Bhagwat, M. J., R. A. Ormiston, H. A. Saberi, and H. Xin, "Application of CFD/CSD Coupling for Analysis of Rotorcraft Airloads and Blade Loads in Maneuvering Flight," Amer. Hel. Soc. 63rd Annual Forum, Virginia Beach, VA, 2007.
15. Saberi, H., M. Khoshlahjeh, R. A. Ormiston, and M. J. Rutkowski, "Overview of RCAS and Application to Advanced Rotorcraft Problems," Amer. Hel. Soc. 4th Decennial Specialist's Conference on Aeromechanics, San Francisco, CA, 2004.
16. Bunning, P., "Consolidation of Time-Accurate, Moving Body Capabilities in OVERFLOW," 6th Overset Composite Grid and Solution Technology Symposium, Ft. Walton Beach, FL, 2002.
17. Bousman, W. G., "A Qualitative Examination of Dynamic Stall from Flight Test Data," *J. Amer. Hel. Soc.*, Vol. 43, (4), 1998, pp. 279-295.
18. Gabel, R., M. Sheffler, F. Tarzanin and D. Hodder, "Wind Tunnel Modeling of Rotor Vibratory Loads," *J. Am. Hel. Soc.*, Vol. 28, (2), 1983, pp. 47-54.
19. Wang, J. M. and J. M. van Aken, "Correlation of Vibratory Hub Loads for a Sikorsky Full-

- Scale Bearingless Main Rotor,” Amer. Hel. Soc. 50th Annual Forum, Washington, D.C., 1994.
20. Wachspress, D. A., T. R. Quackenbush and A. H. Boschitsch, “Rotorcraft Interactional Aerodynamics Calculations with Fast Vortex/Fast Panel Methods,” Amer. Hel. Soc. 56th Annual Forum, Virginia Beach, VA, 2000.
  21. Jacklin, S.A., S. Swanson, A. Blaas, P. Richter, D. Teves, G. Niesl, R. Kube, B. Gmelin and D. L. Key, “Investigation of a Helicopter Individual Blade Control (IBC) System in Two Full-Scale Wind Tunnel Tests: Volume 1,” NASA/TP-2003-212276, 2003.
  22. Torok, M. S., “Aeroelastic Analysis of Active Rotor Control Concepts for Vibration Reduction,” Amer. Hel. Soc. 52nd Annual Forum, Washington, D.C., 1996.
  23. Kottapalli, S., “Calculation of Hub Loads at Low Airspeeds with Active Control,” Amer. Hel. Soc. 63rd Annual Forum, Virginia Beach, VA, 2007.
  24. Corso, L. M., D. A. Popelka, and M. W. Nixon, “Design, Analysis, and Test of a Composite Tailored Tiltrotor Wing,” Amer. Hel. Soc. 53rd Annual Forum, Virginia Beach, VA, 1997.
  25. Peterson, R. L. and W. Johnson, “Aeroelastic Loads and Stability Investigation of a Full-Scale Hingeless Rotor,” International Forum on Aeroelasticity and Structural Dynamics, Aachen, Germany, 1991.
  26. Britton, R. K., “Development of an Analytical Method to Predict Helicopter Main Rotor Performance in Icing Conditions,” AIAA-92-0418, AIAA 30th Aerospace Sciences Meeting, Reno, NV, 1992.
  27. Flemming, R. J. and D. A. Lednicer, “High Speed Ice Accretion on Rotorcraft Airfoils,” NASA CR-3910, August 1985.